FUDMA Journal of Sciences (FJS)
ISSN online: 2616-1370
ISSN print: 2645 - 2944
Vol. 5 No. 3, September, 2021, pp 169 - 176
DOI: https://doi.org/10.33003/fjs-2021-0503-694

CHARACTERIZATION OF HYBRID-FORMAMIDINIUM BISMUTH BROMIDE PEROVSKITE MATERIAL ($FABi_2Br_9$) SYNTHESIZED VIA GROWTH ASSISTED TECHNIQUE FOR SOLAR CELLS APPLICATION

Bashir Salisu

Department of Basic and Applied sciences, College of Science and Technology
Hassan Usman Katsina Polytechnic, katsina, Nigeria.

Corresponding author's email: fatminmed@gmail.com

ABSTRACT

In the last decade, organic-inorganic perovskite solar cells (PSCs) have had tremendous success, raising their power conversion efficiency from 3.8% in 2009(T, A, K, & Y, 2009) to >25.6% (Li *et al*., 2021). Perovskite material is newly emergent, third-generation solar cells, it generally refers to any composite that has structure like that of calcium titanium oxide ($CaTiO_2$). It has a general formula ABX_3, where A refers to an organic compound, B is an inorganic and X represents the halides. In this research, a Hybrid-Formamidinium Bismuth Bromide Perovskite solar cell ($FABi_2Br_9$) was synthesized via a novel crystal growth process and subjected to characterization for determining its optoelectronic properties for solar cells application. The x-ray diffraction (XDR) results revealed the crystal hexagonal structure of $FABi_2Br_9$, the crystal sizes were obtained and it gives an excellent size (74nm) for light absorption material. The bandgap was determined using ultraviolet-visible spectroscopy (U.V vis) which was found to be 1.80eV which is within the required range for an absorbing layer in a solar cell architecture. Nuclear magnetic resonance (NMR) and was used to identify the organic content purity of the composite. In conclusion, $FABi_2Br_9$ was found to be pure with excellent optoelectronics properties that can readily be used as an absorbent layer in perovskite solar cells architecture.

Keywords: Perovskite solar cell, synthesis, characterization, hybrid organic-inorganic, optoelectronics properties, $FABi_2Br_9$, ABX_3 structure.

INTRODUCTION

The universe is drive-by energy; every part of our life involves the utilization of energy. Our automobiles, trains, and boats are all propelled by energy, it can be used to cooks or bakes our food, among other things. Nowadays the energy consumption is increasing and it plays a vital role in the development of the human society. The population of the world is increasing and so is the demand for energy. More than 80% of the world population is living in developing countries, and they are trying to boost their living standards, and this results in higher energy consumption (Vidal-Amaro, *et al.*, 2015).

The use of energy sources like fossil fuels generates problems such as the greenhouse effect, air pollution, global warming, etc. Therefore, the search for new sustainable energy sources is very important and inevitable.

Perovskite solar cell is one of the Photovoltaic (PV) devices, that convert energy from light into electricity. PV devices are based on semiconductor materials, which are defined by an electronic resistivity between metals and insulators. The properties attributed to semiconductors are a result of their electronic band structure. Electrons in a crystalline material have a set of "allowed" energies that form continuous bands separated by forbidden energy levels, due to their periodic crystal lattice. In insulators, all energy levels in a given band are either empty or filled with electrons whereas in metals there are partially filled bands, allowing for electrons to move between states within a band. Semiconductors, in contrast, have multiple bands which are partly filled or partially empty at room temperature, and the ability for carriers to gain or lose energy to move between bands allows for many of the interesting properties of these materials. (Figure 1) In semiconductors, the highest mostly-filled energy band is called the valence band and the lowest mostly-empty energy band is called the conduction band. The difference between the highest energy in the valence band and the lowest energy in the conduction band is the bandgap of the material.

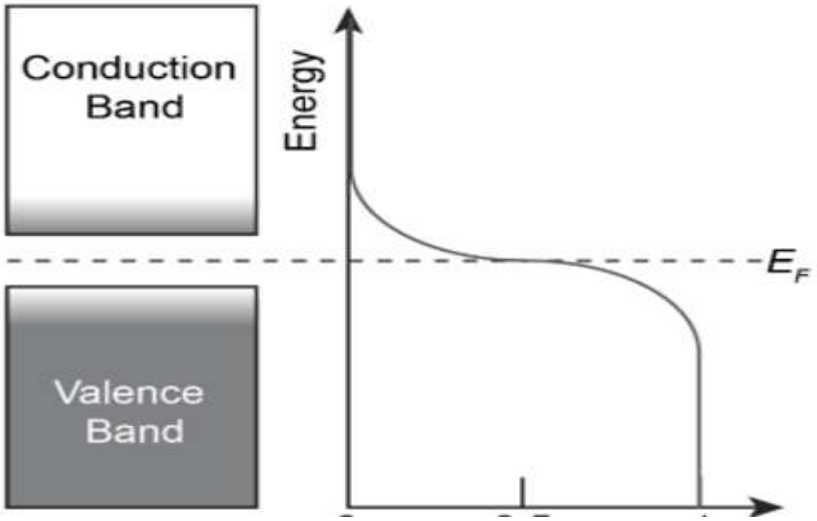

Figure 1. Semiconductor energy levels**.** (Izquierdo, *et al*.,2020)

Perovskite Materials.

Perovskite is a substance with the same crystal structure as the first-discovered perovskite crystal, calcium titanium oxide ($CaTiO_2$). ABX_3 is the chemical formula for perovskite compounds, where A and B are cations and X is an anion that serves as a neutral agent to the A and B cations repulsion. Perovskite structures can be created by combining a variety of different components. Scientists can construct perovskite crystals with a wide range of physical, optical, and electrical properties using this compositional freedom. Ultrasound machines, memory chips, and now solar cells all use perovskite crystals.

.

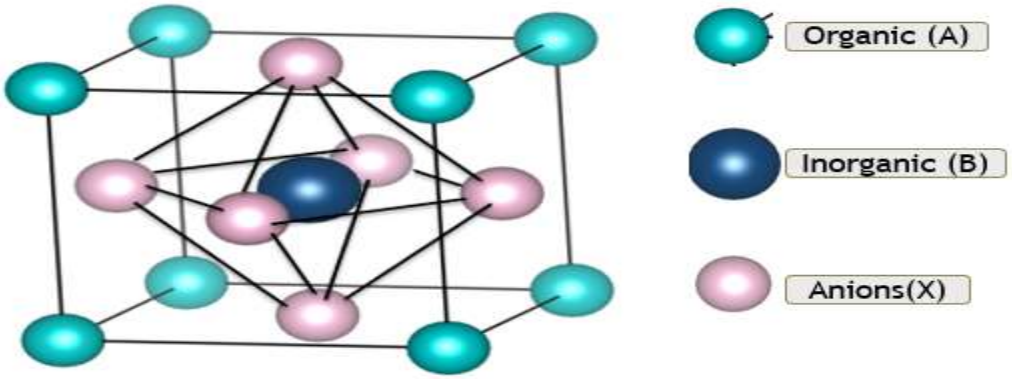

Figure 2. Perovskite structure Drawn using vesta software.

Using lead halide perovskites as the light-absorbing layer, researchers first discovered how to build a stable, thin-film perovskite solar cell with light photon-to-electron conversion efficiency exceeding 10% in 2012 (Sani, *et al.*, 2018). Since then, the efficiency of perovskite solar cells in converting sunlight to electricity has risen, with the laboratory record standing at 25.2 percent. Researchers are also merging perovskite solar cells with ordinary silicon solar cells; current record efficiencies for these "perovskite on silicon" tandem cells are 29.1% ,surpassing the previous record of 27% (Lang *et al.*, 2020) and climbing rapidly. Perovskite solar cells and perovskite tandem solar cells may soon become low-cost, high-efficiency alternatives to conventional silicon solar cells.

To alleviate worries about lead toxicity, researchers are also looking into alternative compositions such as bismuth (Bi^{3+}), tin (Sn^{2+}), germanium (Ge^{2+}) etc to replace lead (Pb^{2+}) due to its health effect and innovative encapsulating techniques for more stability to the perovskite. In this research Bismuth was chosen as a central layer and bismuth perovskites generally have the chemical formula $A_3Bi_2X_9$ (Miller and Bernechea, 2018). Hence the research composite formula is given by $FA_3Bi_2Br_9$.

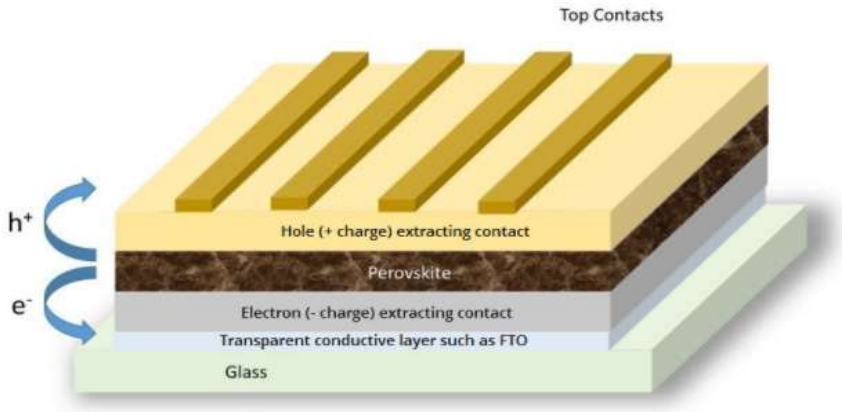

Figure 3. A cross-section of a perovskite solar cell. (Clean Energy Institute, University of Washington)

The outstanding efficiency performance of perovskite halide in photovoltaic devices is made possible through **excellent light absorption**, and this depends on its good morphology which responds to light quickly due to its wide range of absorption (300nm to 850nm) which covers visible light and infrared, and this really enhanced the efficiency.

Another semiconducting property possess by halide perovskite is a long real **charge-carrier** diffusion length, L, ranges from 5 to10 micro-meter (μm), which greatly influence the **lifetime, τ** of the electron to last up to 1 micro-second (μs) when moving from valence band to conduction band before it turns back to the valence band for more energy in single crystal and polycrystalline structure. This process led to the ability of the halide perovskite's bandgap to be tune, which enhanced the efficacy of the perovskite.

Halide perovskite has a high product of the charge carrier mobility (μ) and lifetime **(τ)** i.e., **"μτ"**.

The diffusion length(L) which give rise to good light absorption is given by

$$\mathbf{L=\sqrt{(D\tau)}} \qquad \mathbf{1}$$

Where D is the carrier diffusion coefficient, and is given by

$$\mathbf{D=(\mu q/kBT)} \qquad \mathbf{2}$$

where q is the electron charge, kB is the Boltzmann constant, and T is the absolute temperature.
Equation 2, indicates that charge carrier mobility multiplies the quantity of electron charge which will enhance the total efficiency of the halide perovskite.
The efficiency of the perovskite solar cells can be calculated using short circuit current (I_{sc}), Open circuit voltage (V_{OV}), Maximum power (P_{max}), Fill Factor (FF) and Input power (P_{in}) (which is normally given by 1kw/m^2) through the following relations

$$\eta = \frac{Pmax}{Pin} \times 100\% \qquad 3$$

$$FF = \frac{Pmax}{Isc \times Voc} \qquad 4$$

$$Pmax = FF \times \mathrm{Isc} \times Voc \qquad 5$$

The efficiency is the n given by:

$$\eta = \frac{FF \times \mathrm{Isc} \times Voc}{Pin} \times 100\% \qquad 6$$

Experimental section

Materials:
In the present work, the raw materials used for synthesizing $FABi_2Br_9$ were; Formamide (CH_3NO, Assay 99.5% Sigma Aldrich), Hydrogen bromide (HBr, Assay 99% Sigma Aldrich) Bismuth III Bromide ($BiBr_3$ purity ≥98% Sigma Aldrich), Methanol (CH_3OH Assay 99% Sigma Aldrich), Ethanol (C_2H_5OH Assay 98% Sigma Aldrich). All the chemicals were used as received without any purification or treatment.

Methodology
The precursor Formamidinium Bromide (FABr) were **first** synthesized using the drying oven-assisted technique, where 12ml of Formamide was added in a 50ml of Absolute ethanol in a 250cl conical flask, followed by 6ml of hydrogen bromide (HBr) drop-wisely while stirring the mixture at 0^0C for 2 hours reaction time. Then the mixture was taken to a drying oven for 6 hours, a grey-white powder was obtained (i.e., FABr).
In the **second** step for synthesizing Hybrid-Formamidinium Bismuth Bromide Perovskite solar cell ($FABi_2Br_9$) nanoparticles,0.9mmol of FABr was collected and dissolved in 10ml of methanol followed by 0.6mmol of BiBr in a 250cl small beaker, the beaker was sealed with parafilm and small punches were made on the seal to evacuate the air bubbles, then the mixture was kept for overnight at room temperature. A yellowish precipitate was obtained, then the mixture was centrifuge and dry for 6 hours at 60^0. The powder was ground and put in a sample bottle for characterization.

Results and Discussion
Characterization
Powder X-ray diffraction (PXRD) patterns of $FABi_2Br_9$ nanoparticle synthesized via growth assisted synthesis method were recorded using an X-ray diffractometer (X'pert Pro, PANAlytical with CuKα radiation (λ=0.154187nm) at 40 kV and 40mA in the 2θ range of 10^0 to 60^0 (fig. 4). The particles size of as-synthesized ($FABi_2Br_9$) was calculated using Williamson and Hall formula. The optical bandgap properties of the sample were deduced from optical measurements that was performed on a Shimadzu UV-Vis-NIR diffuse reflectance spectrophotometer (Shimadzu-UV3600). A Nuclear magnetic resonance spectrometer (400 MHz JEOL JNM ECS400) was used to identify the organic compound purity of the composite.

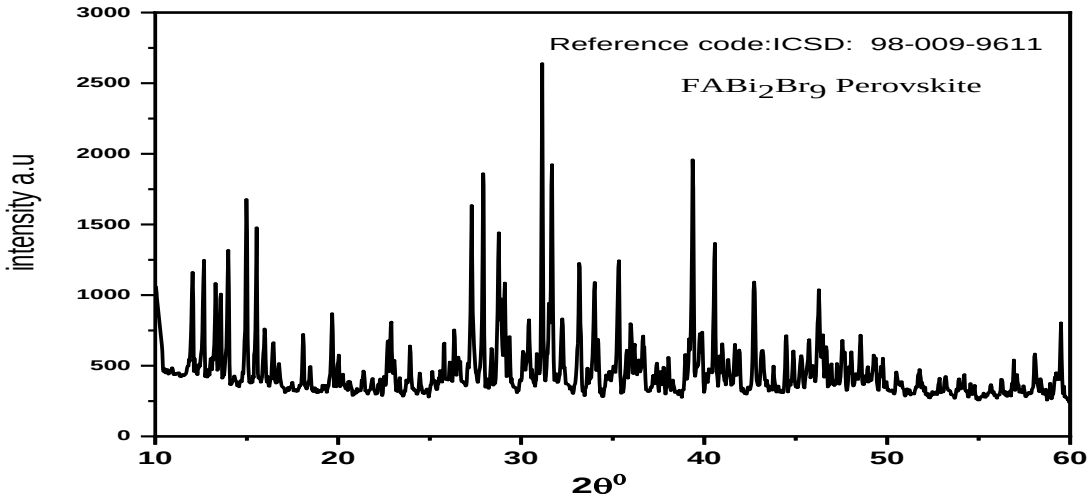

Figure 4. X-Ray Diffraction pattern of $FABi_2Br_9$ nanocrystal.

XRD spectra show the crystal pattern of the as-prepared $FABi_2Br_9$ nanoparticles synthesized via drying oven assisted synthesis method concentrations. The crystal structure, phase, and purity of the as-prepared $FABi_2Br_9$ were determined. Formation of the diffraction peaks revealed the crystalline nature of the as-prepared $FABi_2Br_9$ with peaks at angles 2θ values of 14.98^0, 19.67^0, 22.89^0, 27.91^0, 31.14^0, 33.19^0, 35.34^0, 39.37^0, 42.37^0, 46.2^0, and 59.49^0 corresponding to the hexagonal structure and space group (R-3) of Formamidinium Bismuth Bromide (Reference code: ICSD: 98-009-9611).

X-ray line broadening is one of the characteristic features of XRD signatures and is measured from the full width half maximum (FWHM) of the diffraction peaks. It is basically due to three factors which include instrumental effects, crystallite size effect and micro-strains (Shafi, et al.,2015). In our line broadening analysis, the instrumental effect is neglected because the same instrument is used so the same error is encountered for all samples. The effect of crystallite size and micro-strain cannot be separated hence we used the Williamson-Hall (W-H) plot to quantify their contributions to line broadening (Lucks et al., 2014). W-H analysis accounts for the contributions of crystallite size and micro-strain to peak broadening when large crystallites and thick films are involved. The FWHM for each $FABi_2Br_9$ peak is determined from a Gaussian fit and used for the W-H analysis. Williamson and Hall formula is given by Equation 2,(Singh et al., 2018).

$$FWHM\cos\theta = \frac{K\lambda}{D} + 4\varepsilon\sin\theta \qquad 7$$

$$\beta\cos\Theta = 4\varepsilon\sin\Theta \quad \frac{K\lambda}{D} \qquad 8$$

where β = *full width half maximum (FWHM)*

$$Y = mx + c \qquad 9$$

Comparing (8) and (9) we have:

$$Y = \beta\cos\Theta,\ m = \varepsilon \text{ and } c = \frac{K\lambda}{D} \qquad 10$$

From equation (4)

$$D = \frac{K\lambda}{C} \qquad 11$$

Where *D* crystallite size, *k is a "shape constant for spherical nanoparticles"* which is given by 0.94, λ is a wavelength of x-rays which is equal to 0.1514 nm and *c* teem as intercept.

Crystallite size can be calculated using analytical method, hence the average of crystallite sizes in this research is obtained from the Williamson-Hall (W-H) approach in equation (7)

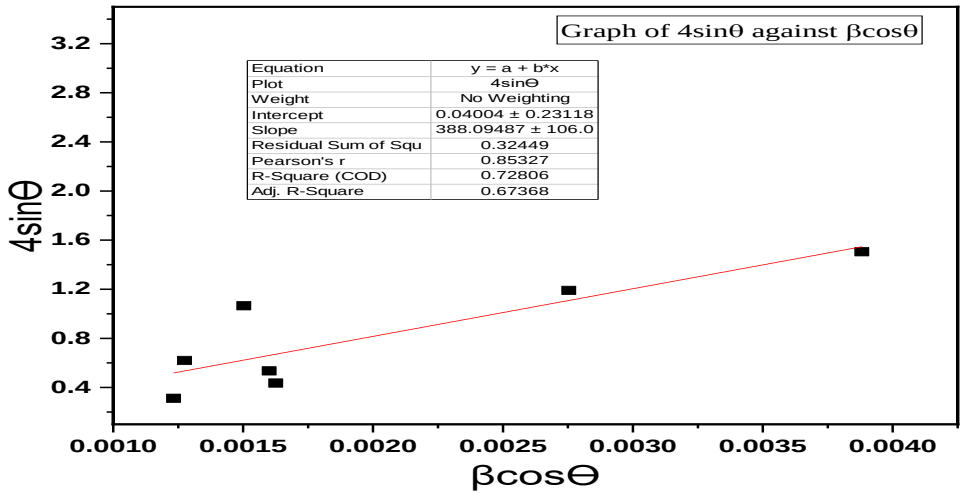

Figure 5. The slope of the Williamson-Hall (W-H) plot 4sinΘ against βcosΘ for $FABi_2Br_9$ diffractogram.

Using equation (11) the crystallite size was calculated to be **74nm** size which corresponds to Scherer's formula value from the expert high score. And this size is within the range of nanocrystal (NCs) ≤ 100nm, which indicates the suitability of the composite for light absorption.

Ultraviolet visible spectroscopy (U.V vis)

The optical bandgap properties of the sample were deduced from optical measurements that was performed using Shimadzu UV-Vis-NIR diffuse reflectance spectrophotometer (Shimadzu-UV3600). The absorption spectra of as-prepared $FABi_2Br_9$ nanoparticles are in the wavelength range of 350nm to 850nm. The as-synthesized product reveals a peak absorption in the wavelength of 735nm. A Similar type of broad absorption was reported by (Ansari et al.,2016)

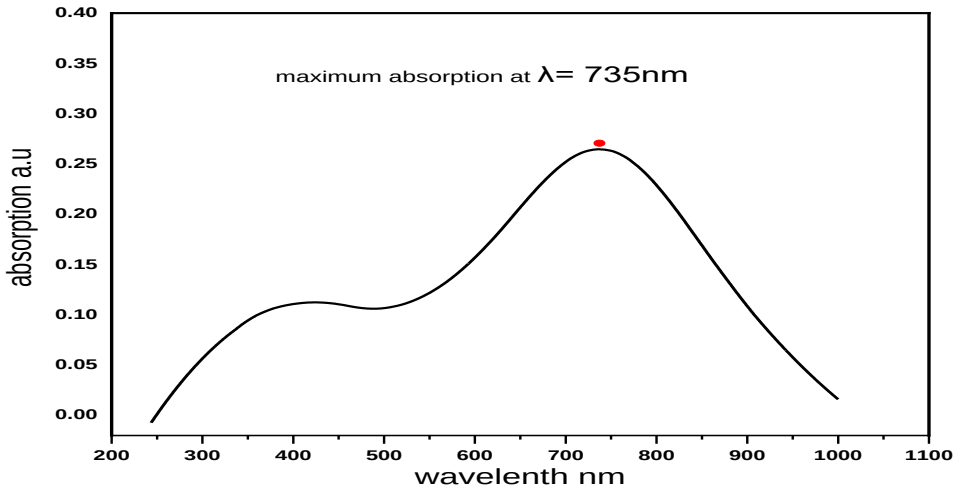

Figure 6. Optical broad absorption of $FABi_2Br_9$

This absorption can be used to calculate the bandgap i.e.

$$Eg = \frac{hv}{\lambda} = \frac{1240}{\lambda} \qquad 12$$

Where *h* is a plank's constant, *v* is the speed of photon and λ_{max} (which is g) is the absorption peak
The bandgap is then 1.7ev using figure 6 and equation 14.
The experimental optical bandgap of $FABi_2Br_9$ NPs was evaluated based on the Kubelka-Munk approach using the following equation;

$$[F(R) * hv\ ]^2 = A\ (hv - E_g) \qquad 13$$

$$F(R) = \frac{K}{S} = \frac{(1-R)2}{2R} \qquad 14$$

The nuclear potential of conductive electrons is significant at a point closer to the Fermi level, which turns out to be quite far from the particle's Centre, and any changes involving permissible quantum numbers will exhibit reduced energy absorption corresponding to the Fermi level energy of the conductive band (Izquierdo et al., 2007).
Using Kubelka-Munk approach by plotting $[F(R) * hv\ ]^2$ against the [F(R) *hv(eV)* (Fig.7) the bandgap is obtained which is equivalent to a bandgap of broad absorption.

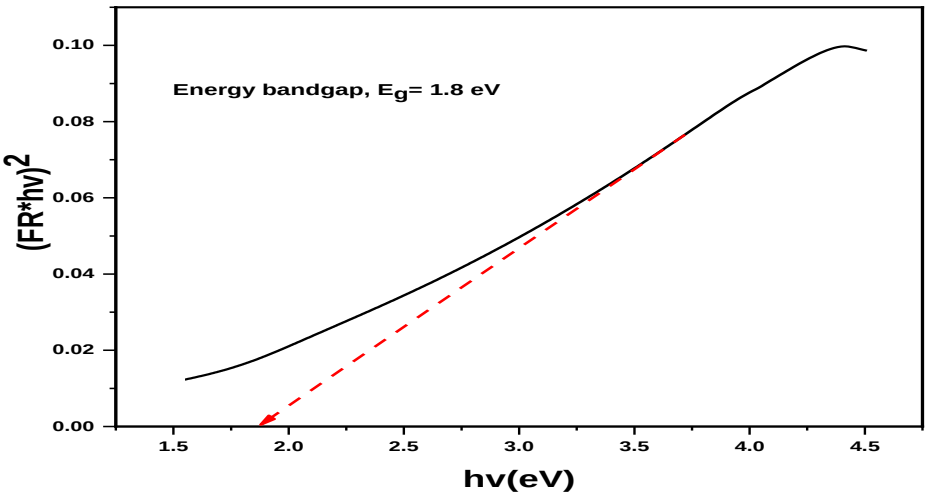

Figure 7. Bandgap calculation using Kubelka-Munk approach.

A Nuclear magnetic resonance spectrometer (400 MHz JEOL JNM ECS400) was used to identify the organic compound purity of the composite.

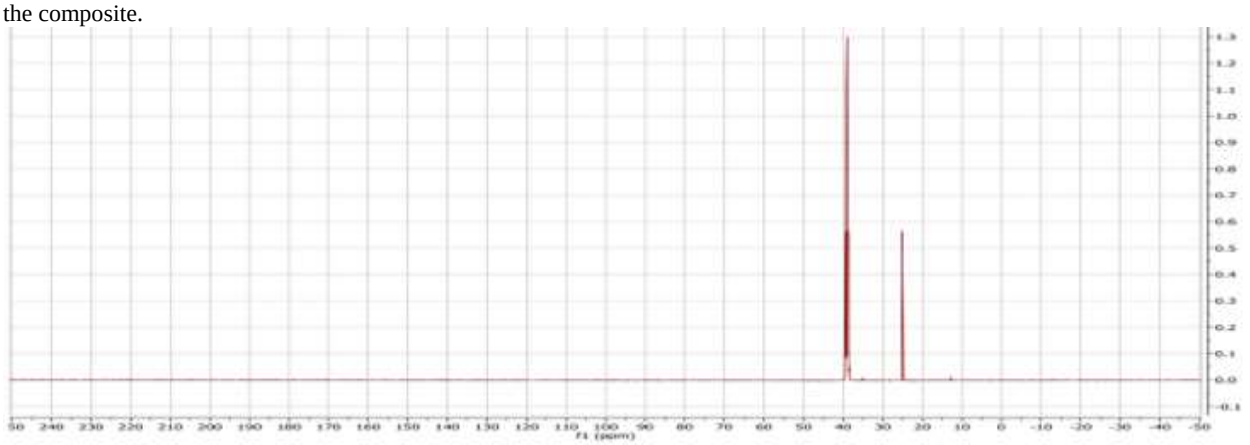

Figure 8. NMR carbon result for $FABi_2Br_9$

The NMR result for carbon in $FABi_2Br_9$ analysis indicates the presence of only one (1) carbon atom at 25.5289ppm. This is confirming that the $FABi_2Br_9$ is in its pure form. While the signal at 39.8447ppm is for the DMSO which is the solvent used.

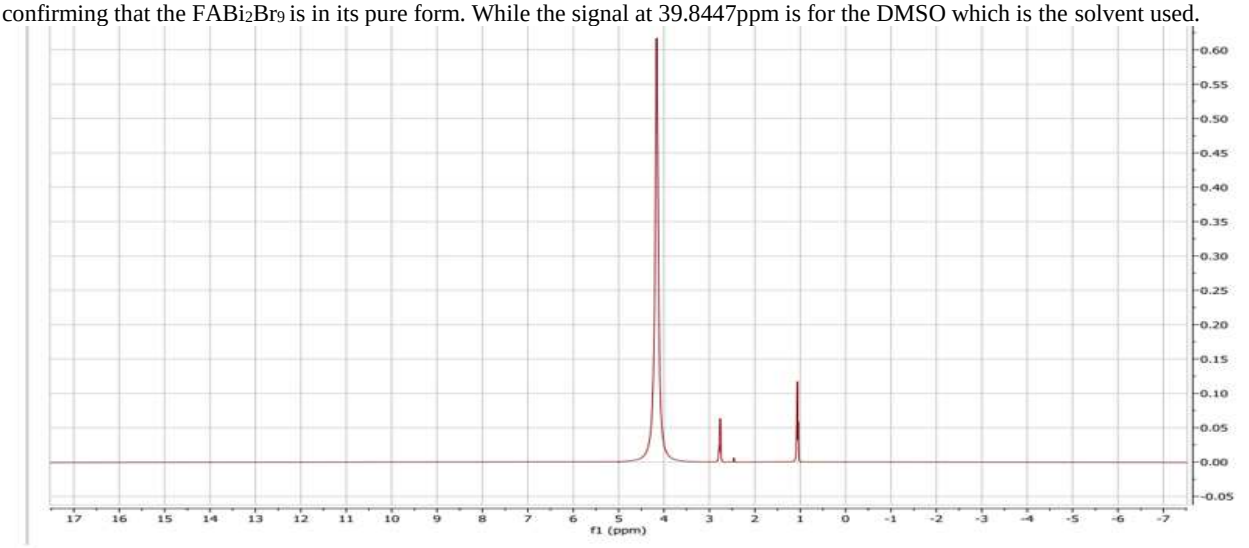

Figure 9. NMR Proton result for $FABi_2Br_9$

NMR Proton result for $FABi_2Br_9$ gives rise to De-shielding chemical shift where multiple peaks of (NH_2), (CH_2) and (CH_2) at a different position. At the range of 2.830 ppm to 2.810 ppm the signal /peak of (H_2) from (NH_2) appear, this is so because the electronegative atom of nitrogen produced more magnetic fields hence reducing the intensity of chemical shift. At 2.810ppm the higher intensity of H_2 from (CH_2) occurred with a split, this is because of its nearness with the electronegative atom of nitrogen. Lastly, the peak of H_3 from (CH_3) appears at 2.77ppm that happened because of its strong chemical shift and less magnetic field. The result shows no moisture presence and the particles are closely parked together.

CONCLUSION

This study highlighted the possibility of using a newly developed method (Growth Assisted Technique) to synthesized an organic-inorganic perovskite layer with excellent optoelectronics properties. The XRD results revealed hexagonal structure of the $FABi_2Br_9$ perovskite with crystallite size of 74nm and a space group of (R-3). The broad absorption revealed the bandgap of 1.7eV which approximately the same as that of kubelka-munk approach (1.8eV). The nuclear magnetic resonance (NMR) indicated the purity of the $FABi_2Br_9$ composite organic content. The observed properties of $FABi_2Br_9$ tally with literature and can be used as an absorbing layer for perovskite solar cells.

REFERENCES

Ansari, A.A., Labis, J., Alam, S.M., Ramay, M., Ahmad, N., Asif, M. (2016) "Influence of copper ion doping on structural, optical and redox properties of CeO_2 nanoparticles."Journal of Electroceramics 36, no. 1-4: 150-157.

Izquierdo, R.V., Alejandro., P.R., Alberto, R.R., Morante, J.R., Lorenzo, C., Bermudez, V.(2007). Raman microprobe characterization of electrodeposited S-rich CuIn $(S,Se)_2$ for photovoltaic applications: microstructural analysis. Journal of applied physics. 101, no. 10 103517.

Shafi, P.M., Bose, A.C. (2015). Impact of crystalline defects and size on X-ray line broadening:A phenomenological approach for tetragonal SnO2 nanocrystals. AIP Adv. 5 057137.

Lucks, I., Lamparter, P., Mittemeijer, E. J. (2014). An evaluation of methods of diffraction-line broadening analysis applied to ball-milled molybdenum Acta Metall. 122–31.

Lang, F., Jošt, M., Frohna, K., Köhnen, E., Al-Ashouri, A., Bowman, A. R., … Stranks, S. D. (2020). Proton Radiation Hardness of Perovskite Tandem Photovoltaics. *Joule*, *4*(5), 1054–1069. https://doi.org/10.1016/j.joule.2020.03.006

Li, J., Duan, J., Yang, X., Duan, Y., Yang, P., & Tang, Q. (2021). Review on recent progress of lead-free halide perovskites in optoelectronic applications. *Nano Energy*, *80*(September 2020), 105526. https://doi.org/10.1016/j.nanoen.2020.105526

Miller, N. C., & Bernechea, M. (2018). Research Update: Bismuth based materials for photovoltaics. *APL Materials*, *6*(8). https://doi.org/10.1063/1.5026541

Sani, F., Shafie, S., Lim, H. N., & Musa, A. O. (2018). Advancement on lead-free organic-inorganic halide perovskite solar cells: A review. *Materials*, *11*(6), 1–17. https://doi.org/10.3390/ma11061008

Singh, R. K., Kumar, R., Kumar, A., Jain, N., Singh, R. K., & Singh, J. (2018). Novel synthesis process of methyl ammonium bromide and effect of particle size on structural, optical and thermodynamic behavior of CH3NH3PbBr3 organometallic perovskite light harvester. *Journal of Alloys and Compounds*, *743*, 728–736. https://doi.org/10.1016/j.jallcom.2018.01.355

T, M., A, K., K, T., & Y, S. (2009). Organometal halide perovskites as visible-light sensitizers for photovoltaic cells. *Journal of the American Chemical Society*, *131*(17), 6050–6051.

Vidal-Amaro, J. J., stergaard, P. A., Sheinbaum-Pardo, C. (2015). Optimal energy mix for transitioning from fossil fuels to renewable energy sources – The case of the Mexican electricity system. Applied Energy, 150, 80-96.

©2021 This is an Open Access article distributed under the terms of the Creative Commons Attribution 4.0 International license viewed via https://creativecommons.org/licenses/by/4.0/which permits unrestricted use, distribution, and reproduction in any medium, provided the original work is cited appropriately.